

Analytical $\pi\pi$ scattering amplitude and the light scalars-II

N.N. Achasov^a and A.V. Kiselev^{a,b}

^a*Laboratory of Theoretical Physics, Sobolev Institute
for Mathematics, 630090, Novosibirsk, Russia*

^b*Novosibirsk State University, 630090, Novosibirsk, Russia*

(Dated: August 10, 2018)

Abstract

In the paper Phys. Rev. **D83**, 054008 (2011) we constructed the $\pi\pi$ scattering amplitude T_0^0 with regular analytical properties in the s complex plane, describing both experimental data and the results based on chiral expansion and Roy equations. Now the results obtained during development of our work are presented. We dwell on questions dealing with the low $\sigma - f_0$ mixing, inelasticity description and the kaon loop model for $\phi \rightarrow \gamma(\sigma + f_0)$ reaction, and show a number of new fits. In particular, we show that the minimization of the $\sigma - f_0$ mixing results in the four-quark scenario for light scalars: the $\sigma(600)$ coupling with the $K\bar{K}$ channel is suppressed relatively to the coupling with the $\pi\pi$ channel, and the $f_0(980)$ coupling with the $\pi\pi$ channel is suppressed relatively to the coupling with the $K\bar{K}$ channel.

The correct analytical properties of the $\pi\pi$ scattering amplitude are reached with the help of rather complicated background function. We also suggest much more simple background parameterization, practically preserving the resonance features, which is comfortable for experimental data analysis, but allows to describe the results based on chiral expansion and Roy equations only on the real s axis.

PACS numbers: 12.39.-x 13.40.Hq 13.66.Bc

I. INTRODUCTION

Study of light scalar resonances is one of the central problems of nonperturbative QCD, it is important for understanding the chiral symmetry realization way resulting from the confinement physics.

In Refs. [1] we described the high-statistical KLOE data on the $\phi \rightarrow \pi^0\pi^0\gamma$ decay [2] in the frame of the kaon loop model $\phi \rightarrow K^+K^- \rightarrow \gamma(f_0 + \sigma) \rightarrow \gamma\pi^0\pi^0$ [3–7] simultaneously with the data on the $\pi\pi$ scattering and the $\pi\pi \rightarrow K\bar{K}$ reaction. The description was carried out taking into account the chiral shielding of the $\sigma(600)$ meson [8, 9] and its mixing with the $f_0(980)$ meson, the data yielded evidence in favor of the four-quark nature of the $\sigma(600)$ and $f_0(980)$ mesons.

At the same time it was calculated in Ref. [10] the $\pi\pi$ scattering amplitude in the s complex plane, basing on chiral expansion, dispersion relations, and Roy equations. In particular, the pole was obtained at $s = M_\sigma^2 = (6.2 - 12.3i) m_\pi^2$, where

$$M_\sigma = 441_{-8}^{+16} - i272_{-12.5}^{+9} \text{ MeV}, \quad (1)$$

which was assigned to the σ resonance. Aiming the comparison of the results of Refs. [1] and [10], we built up the S-wave $\pi\pi$ scattering amplitude T_0^0 with $I = 0$ with correct analytical properties in the complex s plane [11]. Remain that in our model the S matrix of the $\pi\pi$ scattering is the product of the "resonance" and "elastic background" parts:

$$S_0^0 = S_0^{0\text{back}} S_0^{0\text{res}}, \quad (2)$$

and we introduced the special $S_0^{0\text{back}}$ parametrization to obtain the correct T_0^0 analytical properties ($S_0^{0\text{res}}$ had correct analytical properties in Refs. [1] already). In Ref. [11] we successfully described the experimental data and the Ref. [10] results on the real s axis using the constructed $\pi\pi$ amplitude, while the σ pole was located rather far from the Ref. [10] result. We assumed that this deviation is caused by approximate character of the Roy equations, that take into account only the $\pi\pi$ decay channel. This question will be discussed below in more details.

In this paper we present the enlarged data analysis. We dwell on the minimization of the $\sigma - f_0$ mixing, that leads to the four-quark scenario for light scalars: the $\sigma(600)$ coupling with the $K\bar{K}$ channel is suppressed relatively to the coupling with the $\pi\pi$ channel, and

the $f_0(980)$ coupling with the $\pi\pi$ channel is suppressed relatively to the coupling with the $K\bar{K}$ channel [12]. Inelasticity is also crucial for the analysis, here we describe the peculiar behavior of the data up to 1.2 GeV.

In Refs. [1, 11] we used the factor P_K , caused by the elastic $K\bar{K}$ background phase, that allows to correct the kaon loop model, suggested in Ref. [3], under the $K\bar{K}$ threshold. Now we investigate how small this correction may be.

The set of new fits and tables is presented in Sec. II. The residues of the $\pi\pi$ scattering amplitude and its resonance part in resonance poles are presented for the first time.

As the analytical background S_0^{0back} is a rather complicated function, in Sec. III we suggest much more simple background parameterization, practically preserving the resonance features, which is comfortable for experimental data analysis, though allows to describe the results of Ref. [10] only on the real s axis.

The conclusion is in Sec. IV.

Note that the S_0^{0res} parameterization and the complicated background parameterization are the same as in Ref. [11]. The modification of the $K\bar{K}$ background phase is described in Sec. II.

II. DATA ANALYSIS, BACKGROUND WITH THE CORRECT ANALYTICAL PROPERTIES ("COMPLICATED" BACKGROUND)

The measure of the $\sigma - f_0$ mixing intensity is the deviation from the ideal picture, when the $\pi\pi$ scattering phase δ_0^0 is equal to 90° at the $\sigma(600)$ mass m_σ , and equal to 270° at the $f_0(980)$ mass m_{f_0} . We require these phases, $\delta_0^0(m_\sigma)$ and $\delta_0^0(m_{f_0})$, to be close to their "ideal" values.

Remain that the background phase of the $K\bar{K}$ scattering, $\delta_B^{K\bar{K}}$, changes the modulus of the $K\bar{K} \rightarrow \pi^0\pi^0$ amplitude under the $K\bar{K}$ threshold, at $m < 2m_K$, in the amplitude $\phi \rightarrow K\bar{K} \rightarrow \pi^0\pi^0\gamma$ [13]. In Ref. [11] we define

$$P_K = \begin{cases} e^{i\delta_B^{K\bar{K}}} & m \geq 2m_K; \\ \text{analytical continuation of } e^{i\delta_B^{K\bar{K}}} & m < 2m_K. \end{cases} \quad (3)$$

In the present paper we investigate the influence of P_K on the $\phi \rightarrow (f_0 + \sigma)\gamma$ amplitude in the $f_0(980)$ region, $m > 850$ MeV. We upgrade the parametrization of the $\delta^{K\bar{K}}(m)$, used

in Refs. [1, 11], now the $\delta_B^{K\bar{K}}$ is parametrized in the following way:

$$e^{2i\delta_B^{K\bar{K}}} = \frac{1 + i2p_K f_K(m^2)}{1 - i2p_K f_K(m^2)}, \quad p_K = \frac{1}{2}\sqrt{m^2 - 4m_{K^+}^2},$$

$$f_K(m^2) = -\left(1 - w + w \frac{(m - m_2)^2/\Lambda_2^2}{1 + (m - m_2)^2/\Lambda_2^2}\right) \frac{\arctan\left(\frac{m^2 - m_1^2}{\Lambda_1^2}\right) - \phi_0}{\Lambda_K}. \quad (4)$$

Note that the P_K also provides pole absence in the analytical continuation of the $\phi \rightarrow (f_0 + \sigma)\gamma$ amplitude under the $\pi\pi$ threshold, see Ref. [1].

The experimental data on the inelasticity η_0^0 , see Fig. 4, favor the low value near 1.01 GeV and sharp growth up to 1.2 GeV. Below it is shown that it is possible to reach such a behaviour.

Our results for Fits 1-5 are shown in Tables I-VI and Figs. 1-24. Fits 1-5 show that the allowed range of $\sigma(600)$ and $f_0(980)$ parameters is rather wide. For example, $g_{f_0K^+K^-}^2/4\pi$ is 1 GeV² in Fit 1 and more than 4 GeV² in Fit 5. This result may be important for coordination of the $g_{f_0K^+K^-}^2/4\pi$ and $g_{a_0K^+K^-}^2/4\pi$ [14].

Note that in Fit 4 the $\sigma(600)$ and $f_0(980)$ are coupled only with the $\pi\pi$ channel and the $K\bar{K}$ channel ($x_{f_0} = x_\sigma = 0$). As seen from Table I and Figs. 9-16, Fit 4 is in excellent agreement with the data and the [10] results.

We introduce 56 parameters, but for restrictions (expresses 5 parameters through others) and parameters (or their combinations), that go to the bound of the permitted range (9 effective links), the effective number of free parameters is reduced to 42. But it is significant that fits describe as the experimental data (65 points), as well as the $\pi\pi$ amplitude from the [10] in the range $-5m_\pi^2 < s < 0.64$ GeV² which is treated along with experimental data.

As in [11] we show resonance poles of the T_0^0 on some unphysical sheets of its Riemannian surface, depending on sheets of the polarization operators $\Pi_R^{ab}(s)$. For this choice of sheets the imaginary parts of pole positions M_R would be connected to the full widths of the resonances ($2\text{Im}M_R = \Gamma_R = \sum_{ab} \Gamma(R \rightarrow ab)$) in case of metastable states, decaying to several channels. Note also that we do not show poles for Fit 2.

One can see that the obtained $\sigma(600)$ pole positions lie far from Eq. (1). In Ref. [11] we noted, that one of the possible reasons is the approximate character of the Roy equations, that take into account only the $\pi\pi$ channel.

Table I. Properties of the resonances and main characteristics are shown.

The resonance masses m_R and widths $\Gamma_R(m_R)$ (which may be called "Breit-Wigner" masses and widths) are parameters in the resonance propagators, see Ref. [11]. They have clear physical meaning in contrast to the resonance poles in the complex plane.

Fit	1	2	3	4	5
m_{f_0} , MeV	978.30	974.78	981.49	979.85	980.40
$g_{f_0K^+K^-}$, GeV	3.54	4.34	5.01	5.01	7.33
$g_{f_0K^+K^-}^2/4\pi$, GeV ²	1	1.5	2	2	4.2782
$g_{f_0\pi^+\pi^-}$, GeV	-1.3924	-1.6150	-1.9836	-1.6455	-2.5874
$g_{f_0\pi^+\pi^-}^2/4\pi$, GeV ²	0.154	0.208	0.313	0.215	0.533
x_{f_0}	0.6367	0.6039	1.1701	0	1.1972
$\Gamma_{f_0}(m_{f_0})$, MeV	56.7	76.6	114.8	79.1	195.5
m_σ , MeV	479.40	471.89	470.87	472.87	469.94
$g_{\sigma\pi^+\pi^-}$, GeV	2.6676	2.6614	2.7190	2.7093	2.7362
$g_{\sigma\pi^+\pi^-}^2/4\pi$, GeV ²	0.564	0.569	0.588	0.584	0.596
$g_{\sigma K^+K^-}$, GeV	0.553	0.101	0.279	0.274	0.149
$g_{\sigma K^+K^-}^2/4\pi$, GeV ²	0.001	0.048	0.006	0.006	0.002
x_σ	1.1822	0.9187	1.7336	0	1.6291
$\Gamma_\sigma(m_\sigma)$, MeV	362.1	363.2	379.5	376.0	384.7
C , GeV ²	0.05120	0.04465	0.01307	0.00167	0.03345
δ , °	-64.69	-58.7	-64.6	-55.4	-44.0
a_0^0 , m_π^{-1}	0.223	0.220	0.224	0.223	0.225
Adler zero in $\pi\pi \rightarrow \pi\pi$	(93.5 MeV) ²	(85.6 MeV) ²	(96.8 MeV) ²	(94.6 MeV) ²	(92.3 MeV) ²
$\delta_0^{0\text{res}}(m_\sigma)$, °	91.8	94.1	91.0	90.6	92.3
$\delta_0^{0\text{res}}(m_{f_0})$, °	250.1	250.1	260.1	255.1	258.7
$\eta_0^0(1010 \text{ MeV})$	0.55	0.52	0.51	0.51	0.51
χ_{phase}^2 (44 points)	53.1	48.9	42.0	40.0	55.1
χ_{sp}^2 (18 points)	21.2	20.8	21.3	17.0	12.6

Table II. Parameters of the $K\bar{K}$ background phase, $\delta_B^{K\bar{K}}$, are shown.

Fit	1	2	3	4	5
Λ_K , GeV	0.975	1.245	1.375	1.450	1.894
Λ_1 , MeV	381.56	404.49	387.56	412.43	322.93
Λ_2 , MeV	83.113	81.137	86.246	65.000	68.041
m_1 , MeV	827.48	823.54	801.40	791.48	808.17
m_2 , MeV	909.17	923.55	911.59	970.52	963.55
w , MeV	0.471	0.618	0.492	0.750	0.750
ϕ_0	-0.299	0.021	0.153	0.271	0.622

As it was shown in the $SU(2)\times SU(2)$ linear σ model, Ref. [9], the residue of the σ pole in the amplitude of the $\pi\pi$ scattering can not be connected to coupling constant in the Hermitian (or quasi-Hermitian) Hamiltonian for it has a large imaginary part. Here we calculate the residues of the amplitude T_0^0 in the $\sigma(600)$ pole, see Table V, and illustrate this fact in our case. Note that large imaginary part is both in the residues of the full amplitude T_0^0 and its resonance part T_0^{0Res} . So, considering the residue of the σ pole in T_0^0 or T_0^{0Res} as proportional to the square of its coupling constant to the $\pi\pi$ channel is not a clear guide to understanding the σ meson nature. In addition, this pole can not be interpreted as a physical state for its huge width.

One can see from Figs. 8b, 16, and 24a that for Fits 2-5 with $g_{f_0K+K-}^2/4\pi \geq 1.5 \text{ GeV}^2$ the maximum of the $|P_K|^2$ is close to 1 (about 1.2), this means that the correction to the kaon-loop model [3] is small. For lower $g_{f_0K+K-}^2/4\pi$ the $|P_K|^2$ increases as a compensation, see Fit 1 and Fig. 8a. This results in a model dependence of the constant determination. A precise measurement of the inelasticity η_0^0 would resolve this problem.

One can see from Table I that for all Fits 1-5 the resonance phase $\delta^{res}(m)$ is close to 90° at m_σ and to 270° at m_{f_0} , see also Figs. 3, 11, and 19a.

Table III. Parameters of the first background ($P_{\pi 1}$), see Ref. [11], are shown.

Fit	1	2	3	4	5
a_1	-2.767	-1.997	-2.727	-3.152	-2.320
a_2	0.00997	0.02824	0.01228	0.00995	0.00987
a_3	0	0	0	0	0
a_4	2.4774	1.1655	1.9460	3.6119	1.9579
α_1, GeV^2	430.875	-3.472	299.566	187.438	230.647
α_2, GeV^4	1038.375	802.006	1006.643	924.912	876.525
α_3, GeV^6	853.500	810.211	840.573	805.455	805.900
α_4, GeV^8	237.251	239.362	232.860	225.823	233.065
$\alpha_5, \text{GeV}^{10}$	25.3514	25.4850	24.8635	24.9756	25.2960
$\alpha_6, \text{GeV}^{12}$	0.248630	0.218526	0.225182	0.240893	0.224103
c_1, GeV	504.558	680.672	543.245	499.429	557.733
c_2, GeV^3	-2745.58	-2246.19	-2532.80	-2395.72	-2484.57
c_3, GeV^5	132.007	176.850	226.617	256.520	191.569
c_4, GeV^7	390.262	379.216	399.808	404.615	394.230
c_5, GeV^9	50.6689	51.7071	50.4545	49.8151	51.4728
c_6, GeV^{11}	-0.612729	-0.636956	-0.633709	-0.711296	-0.646822
m_1, MeV	921.52	766.81	1049.46	1088.06	915.18
g_1, MeV	301.06	302.40	302.30	333.34	330.83
m_2, MeV	1395.84	937.07	970.74	1104.06	1025.77
g_2, MeV	367.05	305.90	310.37	421.12	324.93
m_3, MeV	1208.42	1432.57	1098.81	1125.51	1330.56
g_3, MeV	335.62	304.46	388.57	378.42	301.39
m_4, MeV	1078.40	898.85	1053.21	1162.64	907.71
g_4, MeV	395.12	429.54	403.00	388.93	437.65
m_5, MeV	1011.58	991.70	1017.19	1051.17	1008.35
g_5, MeV	499.99	503.50	507.03	500.41	502.24
m_6, MeV	932.07	1240.82	1174.80	1154.23	1264.43
g_6, MeV	535.90	616.91	574.55	542.66	629.02

Table IV. Parameters of the second background (P_{π_2}), see Ref. [11], are shown.

Fit	1	2	3	4	5
Λ , MeV	88.506	78.187	73.302	70.443	68.804
k_2	0.0295157	0.0310661	0.0313951	0.0415406	0.0250125
β	143.367	132.832	125.729	126.711	165.179
γ_1	383.759	330.693	365.564	374.814	450.415
γ_2	21.5451	24.7134	22.9274	22.1454	23.1322
m_{1A} , MeV	687.75	668.05	721.92	837.74	607.47
g_{1A} , MeV	301.22	303.07	305.36	392.13	343.56
m_{2A} , MeV	495.44	554.28	492.36	487.79	515.18
g_{2A} , MeV	504.69	488.58	457.53	454.08	494.25
m_{3A} , MeV	631.67	637.64	625.43	599.93	675.83
g_{3A} , MeV	117.86	101.74	101.00	101.35	100.98

Table V. The $\sigma(600)$ poles (in MeV), the residues of T_0^0 , $\text{Res } T_0^0$, and of the resonance part T_0^{0Res} , $\text{Res } T_0^{0Res}$, (in 0.01 GeV^2) in this pole on different sheets of the complex s plane depending on sheets of polarization operators $\Pi^{ab}(s)$ are shown.

Sheets of Π^{ab}					Fit 1			Fit 5		
$\Pi^{\pi\pi}$	$\Pi^{K\bar{K}}$	$\Pi^{\eta\eta}$	$\Pi^{\eta\eta'}$	$\Pi^{\eta'\eta'}$	σ pole	$\text{Res } T_0^0$	$\text{Res } T_0^{0Res}$	σ pole	$\text{Res } T_0^0$	$\text{Res } T_0^{0Res}$
II	I	I	I	I	$565 - 204i$	$-2 + 14i$	$-22 - 11i$	$566 - 201i$	$-1 + 13i$	$-20 - 12i$
II	II	I	I	I	$612 - 346i$	$5 + 3i$	$-18 + 14i$	$569 - 267i$	$3 + 10i$	$-26 - 1i$
II	II	II	I	I	$542 - 396i$	$-1 + 3i$	$-16 - 3i$	$522 - 379i$	$-2 + 3i$	$-14 - 6i$
II	II	II	II	I	$577 - 522i$	$0.2 + 1i$	$-15 - 1i$	$612 - 626i$	$0.3 + 0.4i$	$-15 - 4i$
II	II	II	II	II	$633 - 534i$	$1 + 1i$	$-23 + 2i$	$664 - 651i$	$0.5 + 0.3i$	$-19 - 4i$
Sheets of Π^{ab}					Fit 3			Fit 4		
$\Pi^{\pi\pi}$	$\Pi^{K\bar{K}}$	$\Pi^{\eta\eta}$	$\Pi^{\eta\eta'}$	$\Pi^{\eta'\eta'}$	σ pole	$\text{Res } T_0^0$	$\text{Res } T_0^{0Res}$	σ pole	$\text{Res } T_0^0$	$\text{Res } T_0^{0Res}$
II	I	I	I	I	$572 - 206i$	$-2 + 14i$	$-21 - 12i$	$579 - 216i$	$-3 + 15i$	$-23 - 12i$
II	II	I	I	I	$572 - 279i$	$3 + 10i$	$-26 + 2i$	$579 - 273i$	$1 + 12i$	$-27 - 1i$
II	II	II	I	I	$526 - 395i$	$-2 + 2i$	$-12 - 5i$	–	–	–
II	II	II	II	I	$623 - 651i$	$0.3 + 0.3i$	$-14 - 3i$	–	–	–
II	II	II	II	II	$683 - 679i$	$1 + 0.1i$	$-19 - 4i$	–	–	–

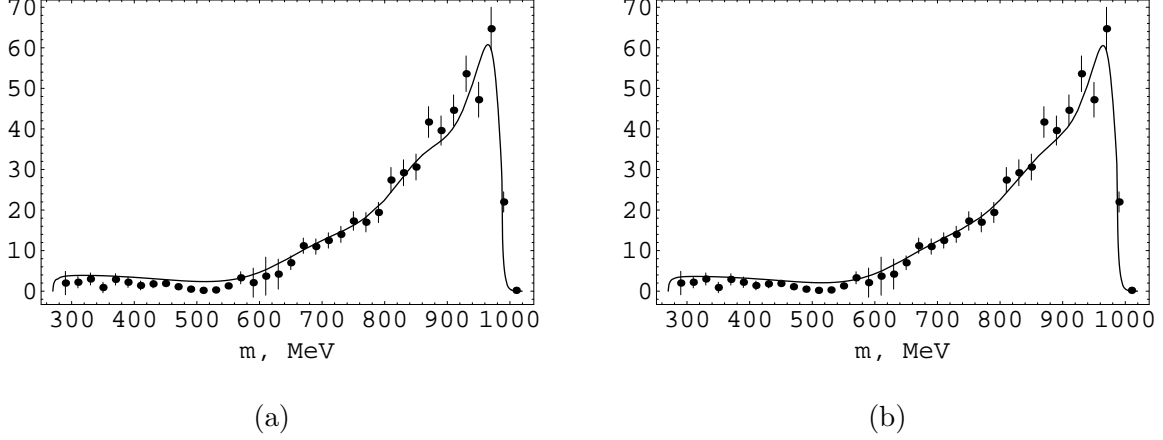
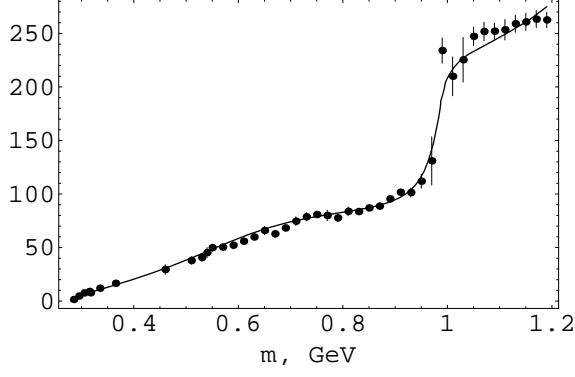


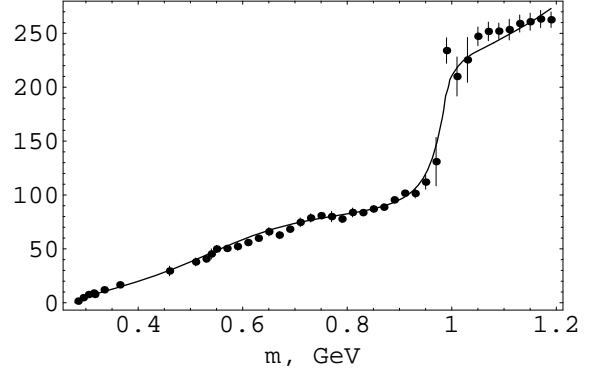
FIG. 1: The $\pi^0\pi^0$ spectrum in the $\phi \rightarrow \pi^0\pi^0\gamma$ decay, theoretical curve, and the KLOE data (points [2]) are shown: a) Fit 1, b) Fit 2.

Table VI. The $f_0(980)$ poles (in MeV), the residues of T_0^0 , $\text{Res } T_0^0$, and of the resonance part T_0^{0Res} , $\text{Res } T_0^{0Res}$, (in 0.01 GeV^2) in this pole on different sheets of the complex s plane depending on sheets of polarization operators $\Pi^{ab}(s)$ are shown.

Sheets of Π^{ab}					Fit 1			Fit 5		
$\Pi^{\pi\pi}$	$\Pi^{K\bar{K}}$	$\Pi^{\eta\eta}$	$\Pi^{\eta\eta'}$	$\Pi^{\eta'\eta'}$	f_0 pole	$\text{Res } T_0^0$	$\text{Res } T_0^{0Res}$	f_0 pole	$\text{Res } T_0^0$	$\text{Res } T_0^{0Res}$
II	I	I	I	I	$986 - 26i$	$6 - 2i$	$-7 + 2i$	$986 - 21i$	$5 - 1i$	$-6 + 0.1i$
II	II	I	I	I	$913 - 302i$	$10 + 5i$	$-19 - 19i$	$1575 - 553i$	$-8 - 4i$	$-21 - 23i$
II	II	II	I	I	$966 - 450i$	$3 - 1i$	$-12 - 10i$	$2101 - 1065i$	$0.1 + 5i$	$-28 - 10i$
II	II	II	II	I	$962 - 465i$	$3 - 0.3i$	$-12 - 12i$	$2173 - 1158i$	$1 + 5i$	$-25 - 11i$
II	II	II	II	II	$954 - 586i$	$1 + 0.4i$	$-3 - 14i$	$2452 - 1570i$	$3 + 3i$	$-22 - 10i$
Sheets of Π^{ab}					Fit 3			Fit 4		
$\Pi^{\pi\pi}$	$\Pi^{K\bar{K}}$	$\Pi^{\eta\eta}$	$\Pi^{\eta\eta'}$	$\Pi^{\eta'\eta'}$	f_0 pole	$\text{Res } T_0^0$	$\text{Res } T_0^{0Res}$	f_0 pole	$\text{Res } T_0^0$	$\text{Res } T_0^{0Res}$
II	I	I	I	I	$986 - 23i$	$6 - 1i$	$-6 + 1i$	$985 - 20i$	$5 - 1i$	$-5 + 1i$
II	II	I	I	I	$1149 - 485i$	$3 - 6i$	$-14 - 16i$	$1187 - 618i$	$0.5 - 2i$	$-11 - 9i$
II	II	II	I	I	$1441 - 835i$	$-3 + 0.4i$	$-20 - 7i$	—	—	—
II	II	II	II	I	$1469 - 885i$	$-2 + 0.4i$	$-16 - 9i$	—	—	—
II	II	II	II	II	$1607 - 1182i$	$-1 + 1i$	$-11 - 8i$	—	—	—

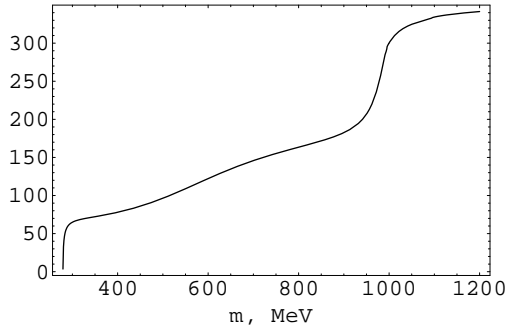


(a)

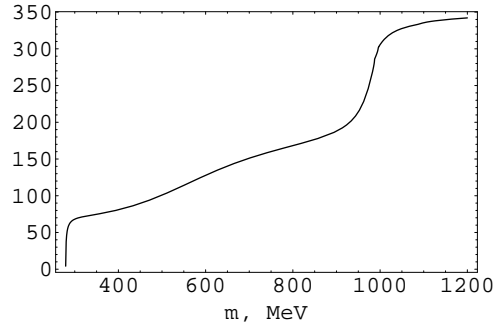


(b)

FIG. 2: The phase δ_0^0 of the $\pi\pi$ scattering (degrees) is shown: a) Fit 1, b) Fit 2. The experimental data from Refs. [15–19].

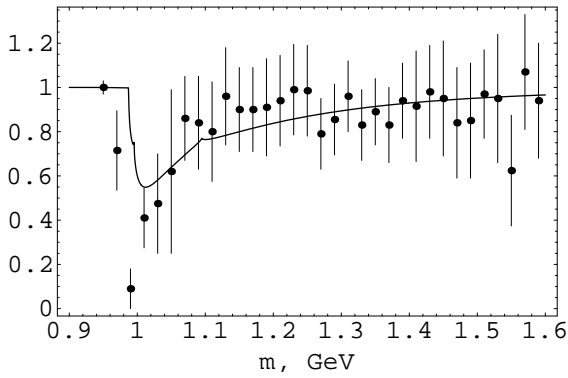


(a)

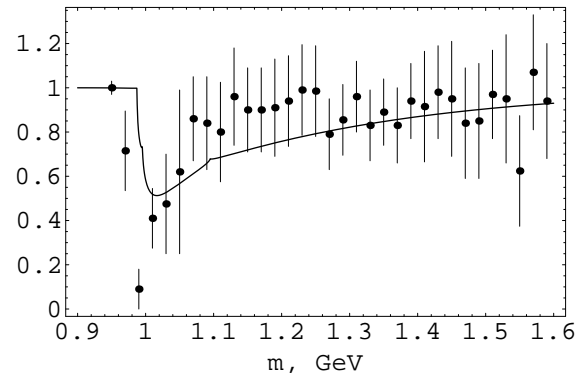


(b)

FIG. 3: The resonance phase of the $\pi\pi$ scattering $\delta_0^{0 res}$ (degrees) is shown: a) Fit 1, b) Fit 2.



(a)



(b)

FIG. 4: The inelasticity η_0^0 is shown: a) Fit 1, b) Fit 2.

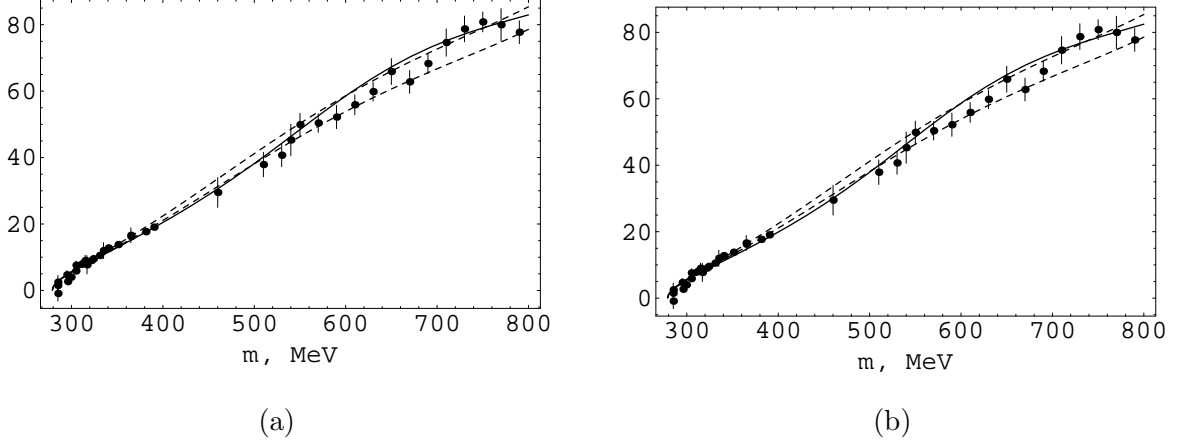


FIG. 5: The phase δ_0^0 of the $\pi\pi$ scattering is shown. The solid line is our description, dashed lines mark borders of the corridor [10], and points are the experimental data from Refs. [15–19, 21, 22]: a) Fit 1, b) Fit 2.

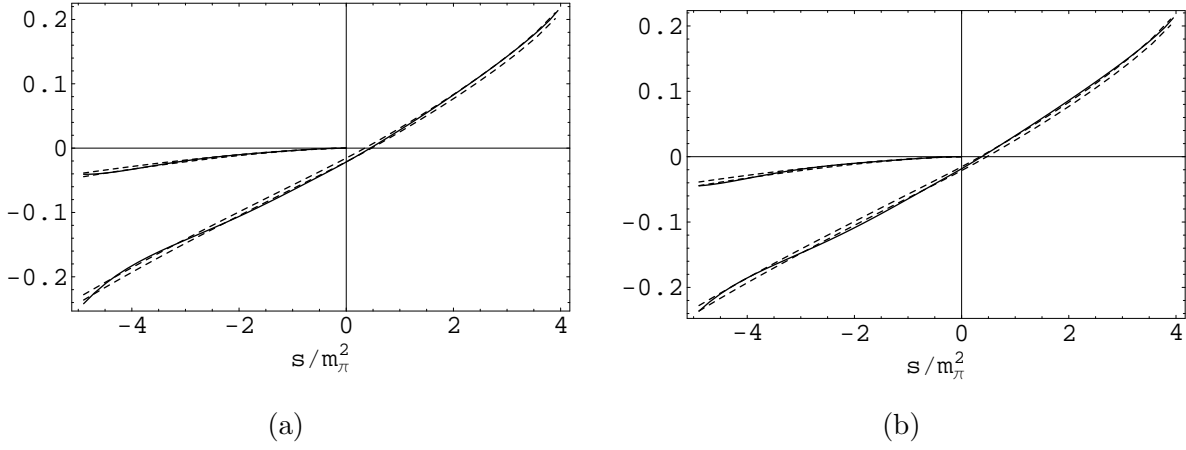


FIG. 6: The real and the imaginary parts of the amplitude T_0^0 of the $\pi\pi$ scattering are shown. Solid lines show our description, dashed lines mark borders of the real part corridor and the imaginary part for $s < 0$ [10]: a) Fit 1; b) Fit 2.

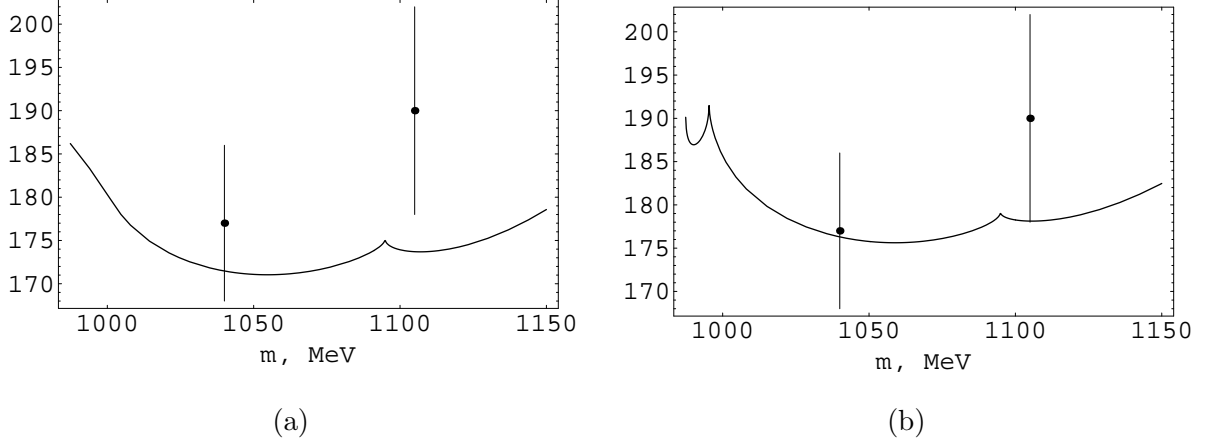


FIG. 7: The phase $\delta^{\pi K}$ of the $\pi\pi \rightarrow K\bar{K}$ scattering is shown: a) Fit 1; b) Fit 2.

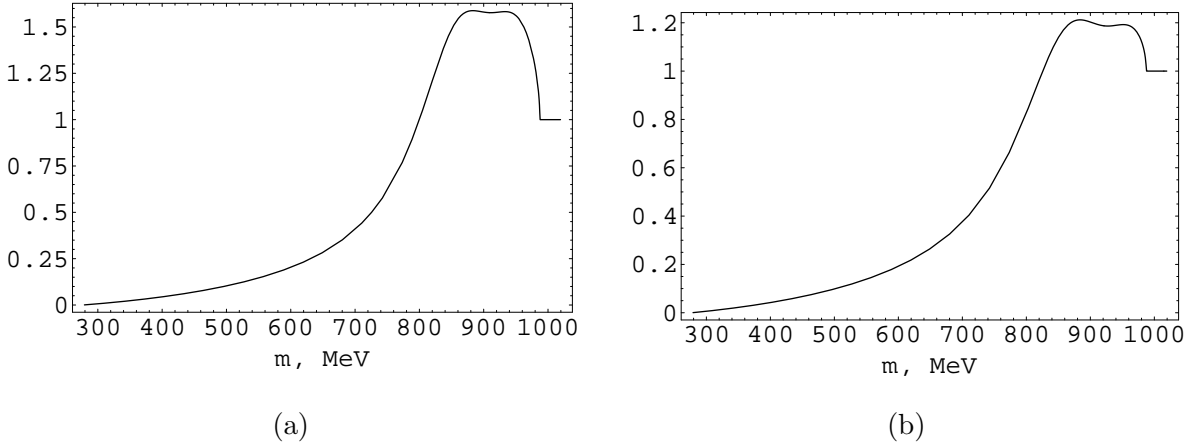


FIG. 8: The $|P_K(m)|^2$ is shown, see Eq. (7): a) Fit 1; b) Fit 2.

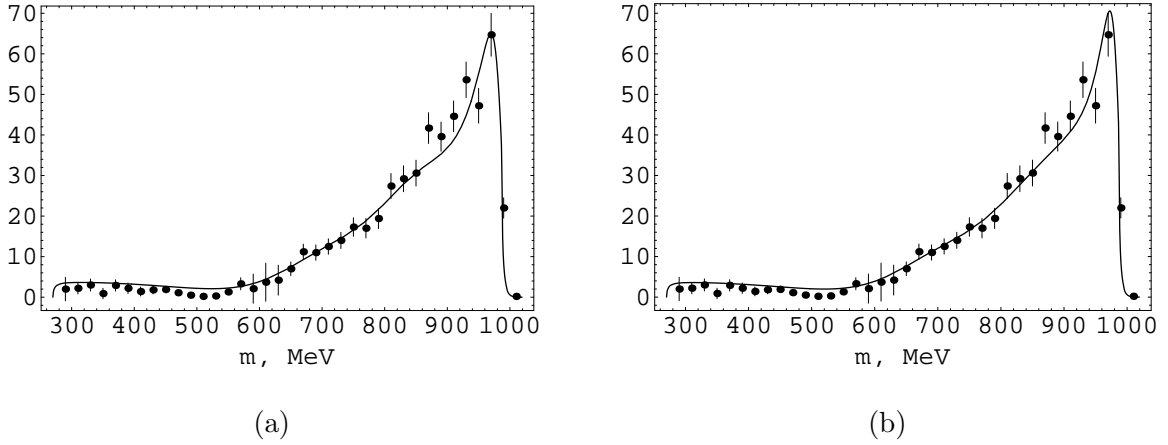
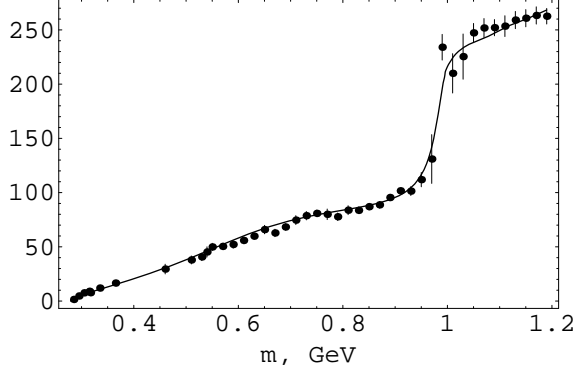
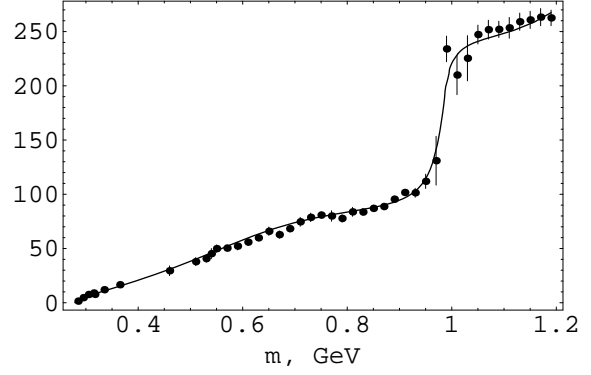


FIG. 9: The $\pi^0\pi^0$ spectrum in the $\phi \rightarrow \pi^0\pi^0\gamma$ decay, theoretical curve, and the KLOE data (points [2]) are shown: a) Fit 3, b) Fit 4.

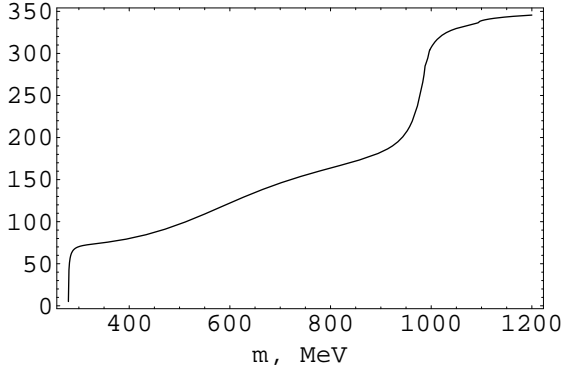


(a)

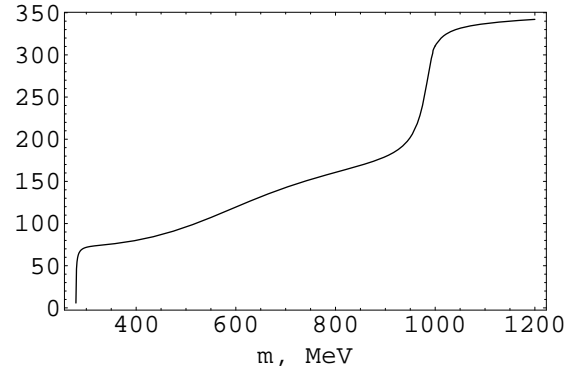


(b)

FIG. 10: The phase δ_0^0 of the $\pi\pi$ scattering (degrees) is shown: a) Fit 3, b) Fit 4. The experimental data from Refs. [15–19].

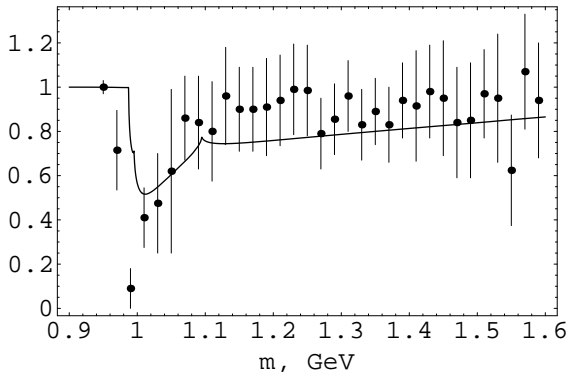


(a)

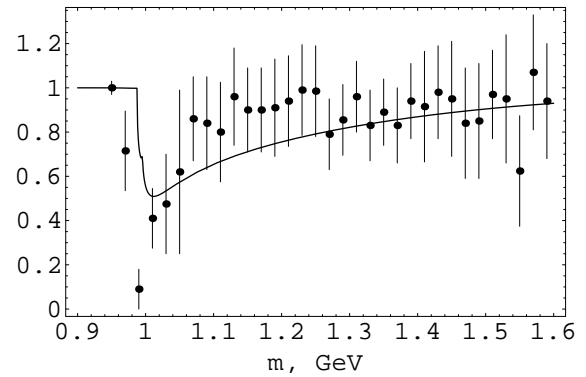


(b)

FIG. 11: The resonance phase of the $\pi\pi$ scattering $\delta_0^{0 res}$ (degrees) is shown: a) Fit 3, b) Fit 4.



(a)



(b)

FIG. 12: The inelasticity η_0^0 is shown: a) Fit 3, b) Fit 4.

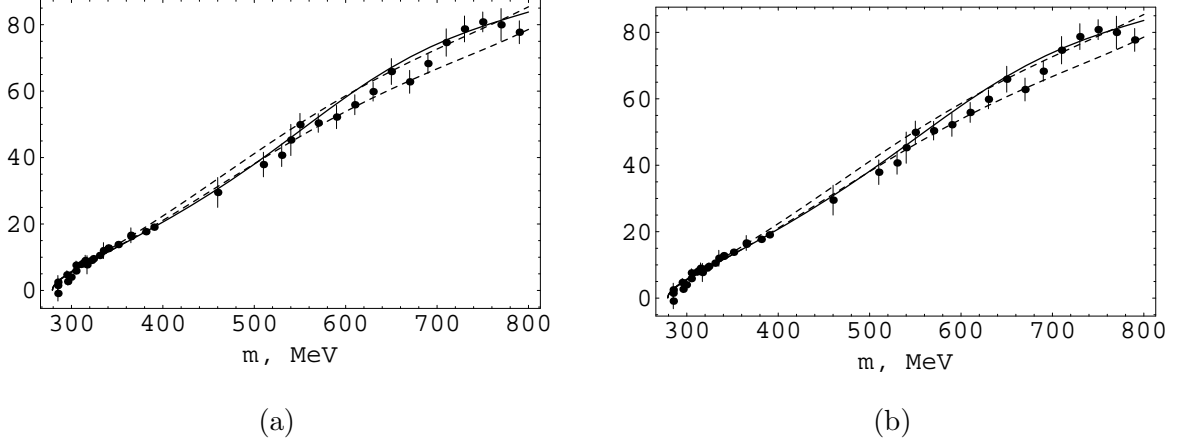


FIG. 13: The phase δ_0^0 of the $\pi\pi$ scattering is shown. The solid line is our description, dashed lines mark borders of the corridor [10], and points are the experimental data from Refs. [15–19, 21, 22]: a) Fit 3, b) Fit 4.

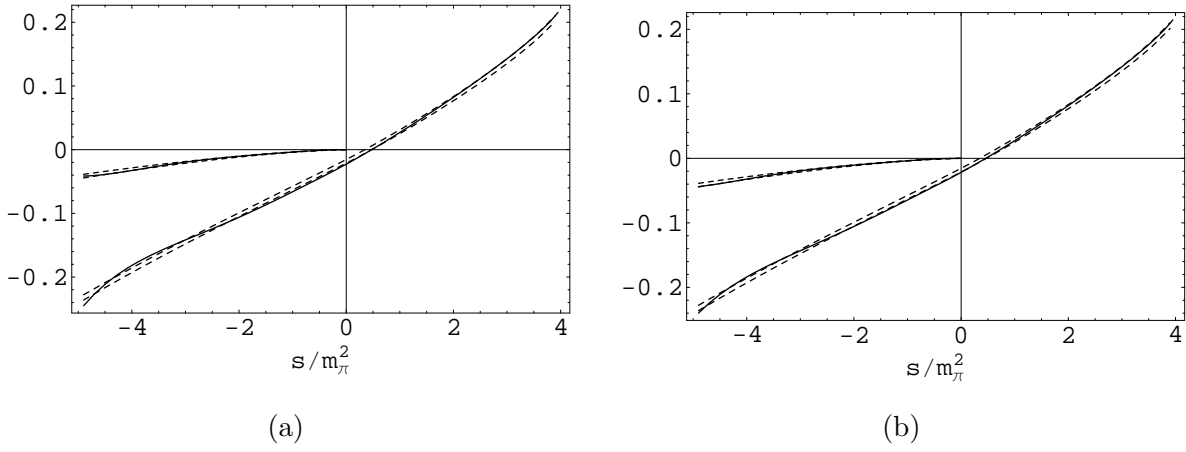


FIG. 14: The real and the imaginary parts of the amplitude T_0^0 of the $\pi\pi$ scattering are shown. Solid lines show our description, dashed lines mark borders of the real part corridor and the imaginary part for $s < 0$ from Ref. [10]: a) Fit 3; b) Fit 4.

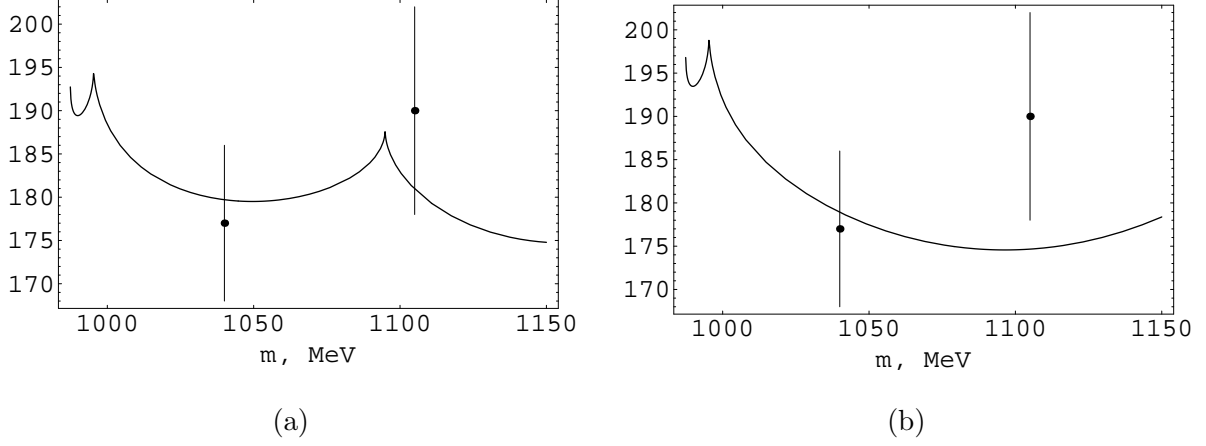


FIG. 15: The phase $\delta^{\pi K}$ of the $\pi\pi \rightarrow K\bar{K}$ scattering is shown: a) Fit 3; b) Fit 4.

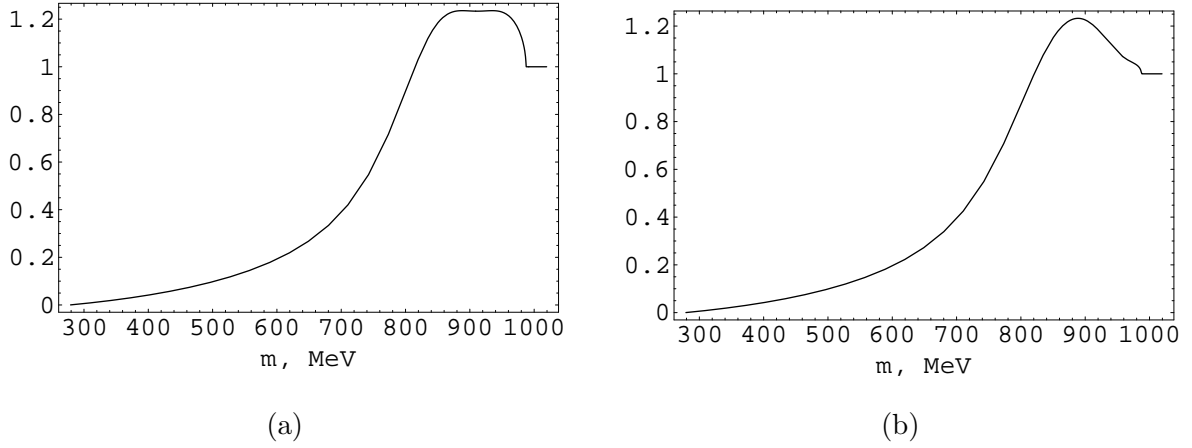


FIG. 16: The $|P_K(m)|^2$ is shown, see Eq. (7): a) Fit 3; b) Fit 4.

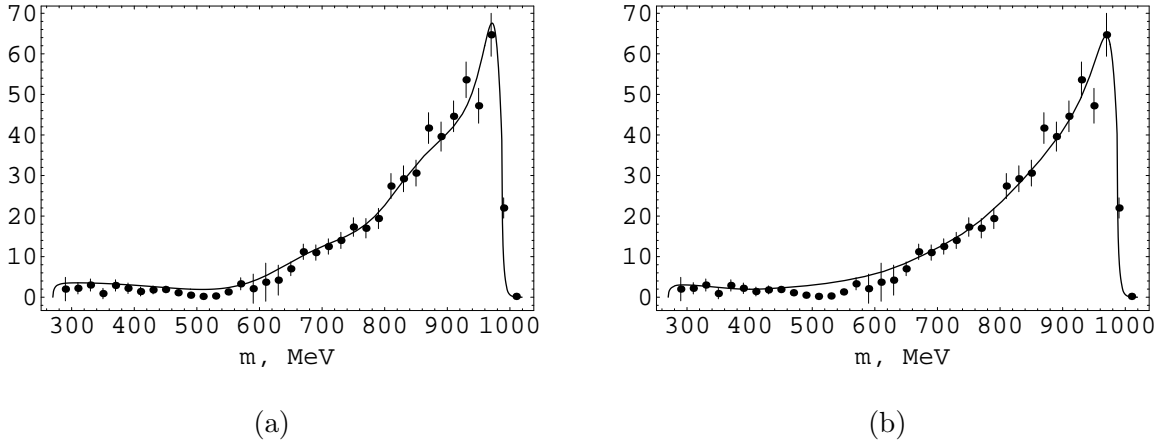


FIG. 17: The $\pi^0\pi^0$ spectrum in the $\phi \rightarrow \pi^0\pi^0\gamma$ decay, theoretical curve, and the KLOE data (points) [2] are shown: a) Fit 5, b) Fit 6.

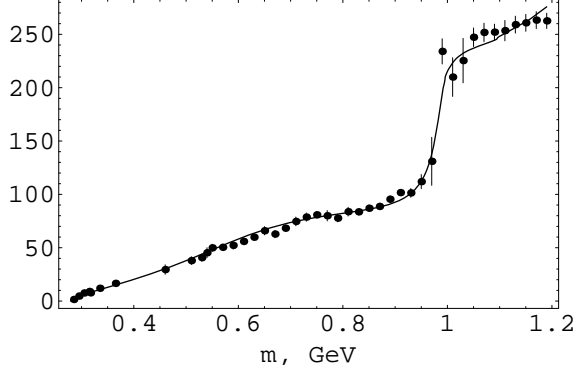
Table VII. Parameters of the Fit 6 (with simple background Eq. (5)).

m_{f_0} , MeV	981.80 ± 1.8	Λ_K , GeV	0.8803
$g_{f_0 K^+ K^-}$, GeV	7.3612	Λ_1 , MeV	490.24
$g_{f_0 K^+ K^-}^2 / 4\pi$, GeV ²	4.3120 ± 1.0	Λ_2 , MeV	154.08
$g_{f_0 \pi^+ \pi^-}$, GeV	-2.3865	m_1 , MeV	754.53
$g_{f_0 \pi^+ \pi^-}^2 / 4\pi$, GeV ²	0.453	m_2 , MeV	422.14
x_{f_0}	0.9875	w , MeV	0.999
$\Gamma_{f_0}(m_{f_0})$, MeV	166.1	ϕ_0	0.787
m_σ , MeV	572.25	b_0	1.41426
$g_{\sigma \pi^+ \pi^-}$, GeV	2.91216	b_1	0.97324
$g_{\sigma \pi^+ \pi^-}^2 / 4\pi$, GeV ²	0.675	b_2	-1.09477
$g_{\sigma K^+ K^-}$, GeV	0.4583	b_3	-0.21134
$g_{\sigma K^+ K^-}^2 / 4\pi$, GeV ²	0.017	c_0	2.48601
x_σ	1.01775	c_1	1.02050
$\Gamma_\sigma(m_\sigma)$, MeV	387.4	c_2	0.45705
C , GeV ²	0.06582	c_3	0.12373
δ , °	-5.8	Λ_1^π	160.84
a_0^0 , m_π^{-1}	0.220	Λ_2^π	522.98
Adler zero in $\pi\pi \rightarrow \pi\pi$	$(89.8 \text{ MeV})^2$	$\delta_0^{0 \text{ res}}(m_\sigma)$, °	93.1
χ_{phase}^2 (44 points)	39.4	$\delta_0^{0 \text{ res}}(m_{f_0})$, °	251.4
χ_{sp}^2 (18 points)	13.9	$\eta_0^0(1010 \text{ MeV})$	0.45

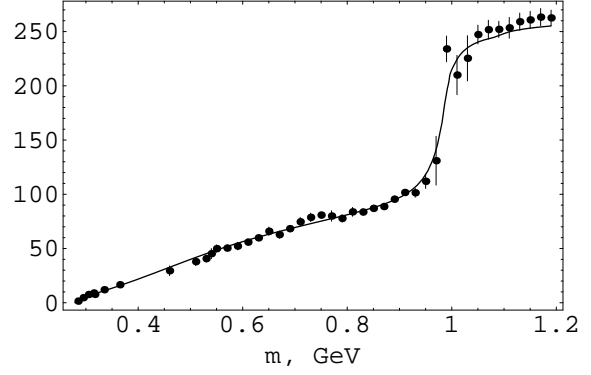
III. SIMPLE BACKGROUND

The background function, suggested in Ref. [11] to reach the correct analytical properties of the $\pi\pi$ scattering amplitude and used above, is rather complicated and costly in computation. In this section we suggest much more simple background parameterization, practically preserving the resonance features, which is comfortable for experimental data analysis and allows to describe the results [10] on the real s axis.

This background function is an upgrade of the one, used in Ref. [1]:

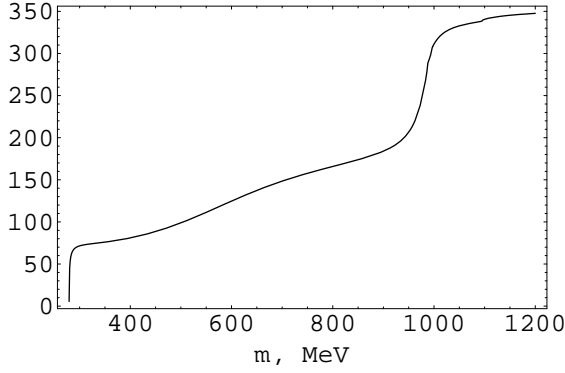


(a)

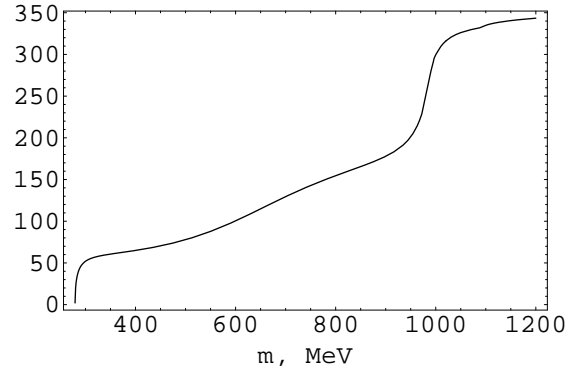


(b)

FIG. 18: The phase δ_0^0 of the $\pi\pi$ scattering (degrees) is shown: a) Fit 5, b) Fit 6. The experimental data from Refs. [15–19].

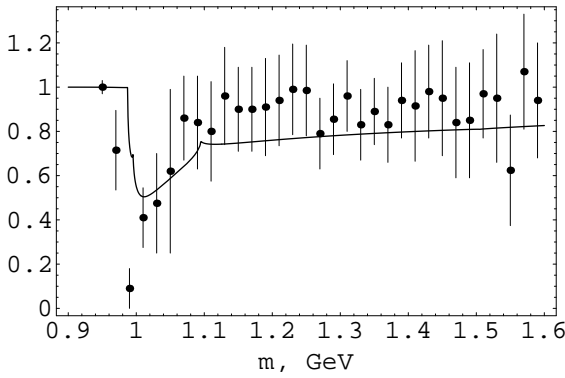


(a)

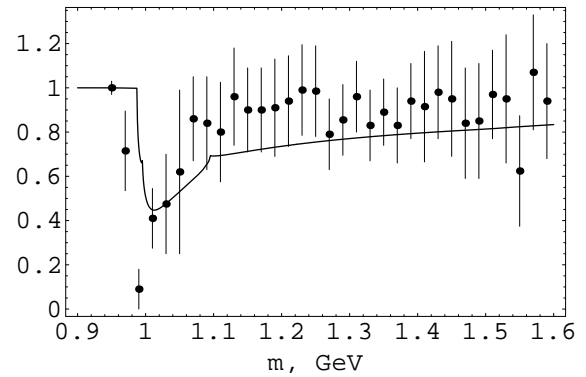


(b)

FIG. 19: The resonance phase of the $\pi\pi$ scattering $\delta_0^{0,res}$ (degrees) is shown: a) Fit 5, b) Fit 6.



(a)



(b)

FIG. 20: The inelasticity η_0^0 is shown: a) Fit 5, b) Fit 6.

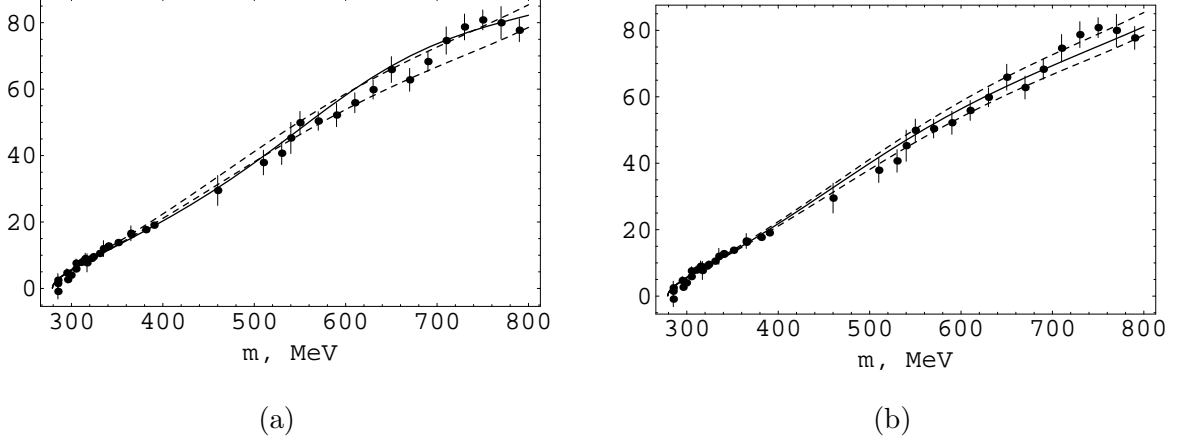


FIG. 21: The phase δ_0^0 of the $\pi\pi$ scattering is shown. The solid line is our description, dashed lines mark borders of the corridor [10], and points are the experimental data from Refs. [15–19, 21, 22]: a) Fit 5, b) Fit 6.

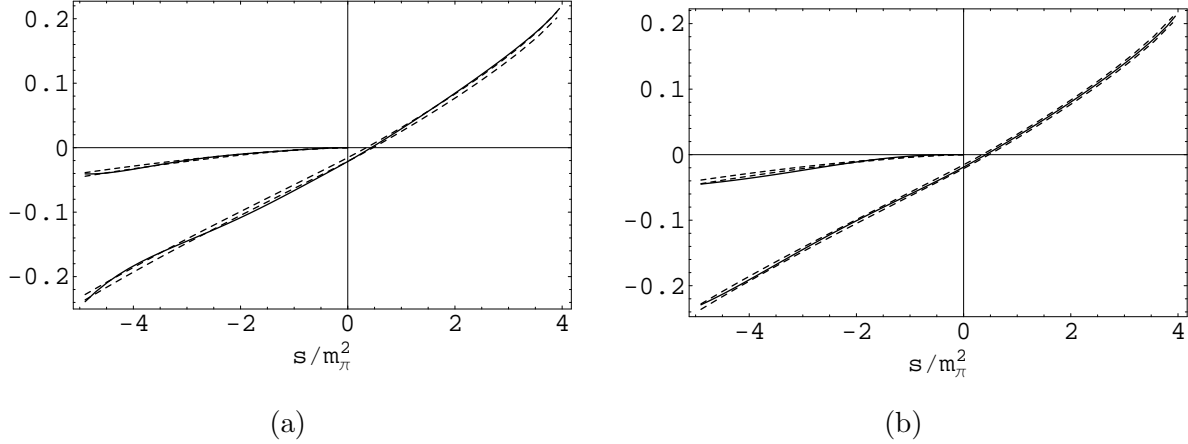


FIG. 22: The real and the imaginary parts of the amplitude T_0^0 of the $\pi\pi$ scattering are shown. Solid lines show our description, dashed lines mark borders of the real part corridor and the imaginary part for $s < 0$ from Ref. [10]: a) Fit 5; b) Fit 6.

$$\tan(\delta_B^{\pi\pi}) = -\frac{p_\pi}{m_\pi} \frac{b_0 - b_1 \frac{p_\pi^2}{m_\pi^2} + b_2 \frac{p_\pi^4}{m_\pi^4} + b_3 \frac{p_\pi^6}{m_\pi^6} + \frac{m}{m_\pi} \left(c_0 + c_1 \frac{p_\pi^2}{m_\pi^2} + c_2 \frac{p_\pi^4}{m_\pi^4} + c_3 \frac{p_\pi^6}{m_\pi^6} \right)}{(1 + 4p_\pi^2/\Lambda_1^{\pi^2})(1 + 4p_\pi^2/\Lambda_2^{\pi^2})}, \quad (5)$$

here $p_\pi = \sqrt{m^2 - 4m_\pi^2}/2$. Note that in comparison with Ref. [1] the function (5) has a left cut.

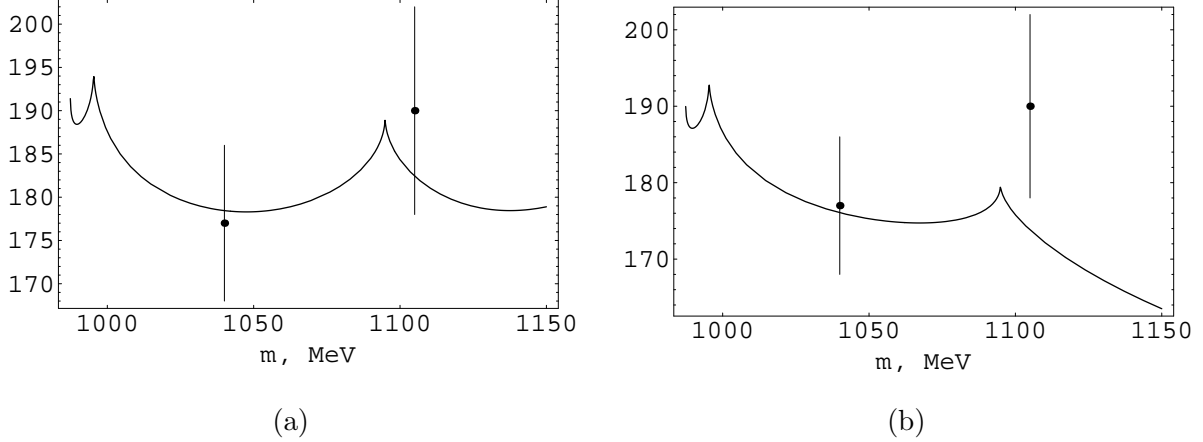


FIG. 23: The phase $\delta^{\pi K}$ of the $\pi\pi \rightarrow K\bar{K}$ scattering is shown: a) Fit 5; b) Fit 6.

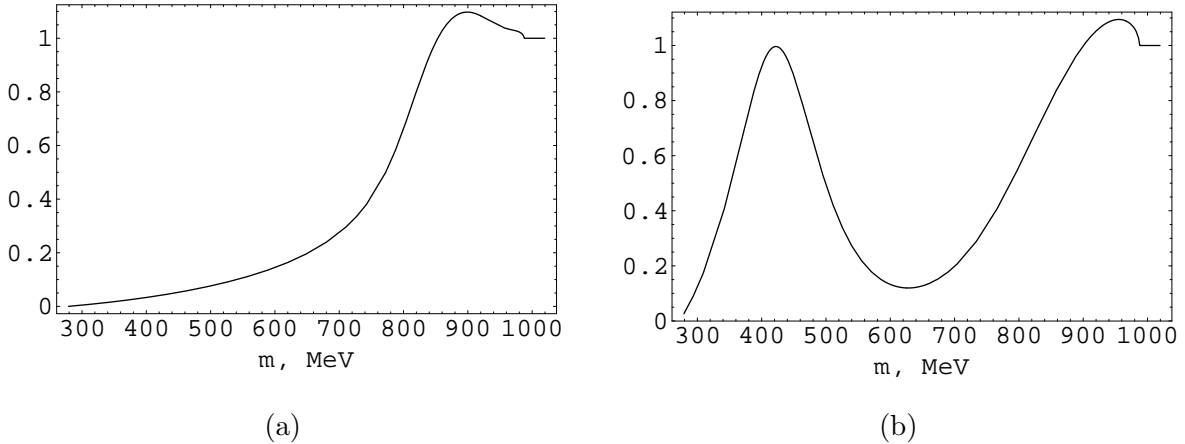


FIG. 24: The $|P_K(m)|^2$ is shown, see Eq. (7): a) Fit 5; b) Fit 6.

Let us build the χ^2 function. It may be divided into 3 parts:

$$\chi^2 = \chi_{data}^2 + \chi_{Roy}^2 + \chi_{restr}^2$$

where the first one is the usual χ^2 function for the experimental data, the second one provides the description of the results [10], and the third one provides the restrictions.

The χ_{data}^2 is constructed with the help of the same data, as in Ref. [11], except the δ_0^0 data in the region $2m_\pi < m < 800$ MeV, where we use the [10] results. Note that in Table I we show χ_{phase}^2 , obtained in the full region $2m_\pi < m < 1200$ MeV with the "old data" [15–19].

The χ_{Roy}^2 caused by the real and imaginary parts of the $T_0^0(m)$ contributions in the region $-5m_\pi^2 < s < 4m_\pi^2$, and the δ_0^0 contribution from the region $4m_\pi^2 < s < (800 \text{ MeV})^2$. Here

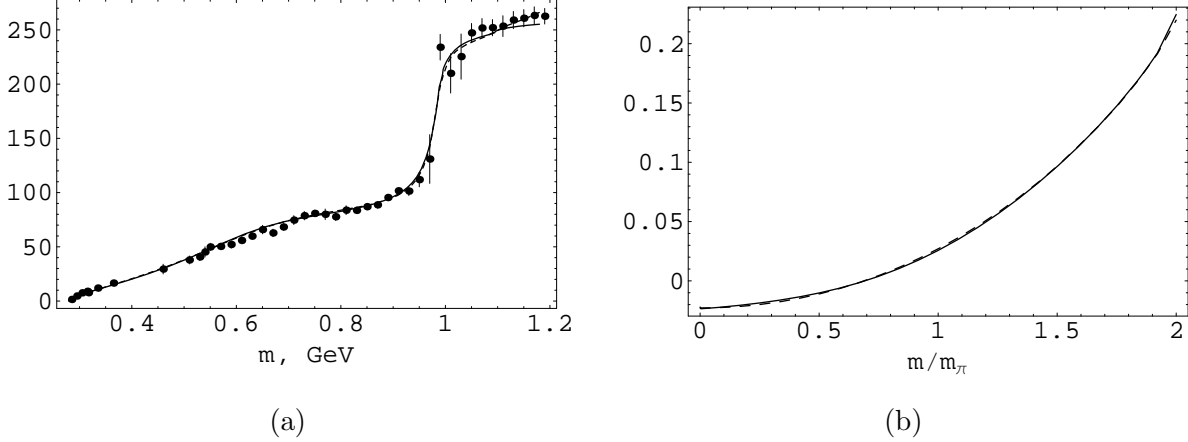


FIG. 25: The comparison of Fit 3 and Fit 7 (with the same resonance parameters, but the background parameterization (5)): a) the phase δ_0^0 , b) the amplitude T_0^0 under the $\pi\pi$ threshold. Solid lines are Fit 7, dashed lines are Fit 3, points are the experimental data. The curves are practically the same.

for ReT_0^0 and δ_0^0 we used points and errors, kindly sent us by H. Leutwyler, and for ImT_0^0 the approximate curve $ImT_0^0(m) = -0.0327(m/2m_\pi)^3$, obtained using Fig. 1 in Ref. [10], providing us with central values, and the error is assumed to be 25%. Note that for ImT_0^0 we used the "reper" points $s = -(30 \text{ MeV})^2, -(50 \text{ MeV})^2, -(100 \text{ MeV})^2, -(150 \text{ MeV})^2, -(200 \text{ MeV})^2, -(250 \text{ MeV})^2, -(280 \text{ MeV})^2, -(308.95 \text{ MeV})^2$, the last is the end of the domain of validity of the Roy equations, connected with the Lehmann-Martin ellipse, see [10].

We impose the following set of restrictions, contributing to χ_{restr}^2 :

- 1) $85^\circ < \delta_0^{0res}(m_\sigma) < 95^\circ$ and $250^\circ < \delta_0^{0res}(m_{f_0}) < 290^\circ$ to provide small $\sigma - f_0$ mixing, a kind of diagonalization that results in the four-quark model scenario.
- 2) $1.2 > |P_K|^2 > 0.8$ for $m > 850 \text{ MeV}$. The maximum is found dynamically (at every calculation of the χ^2 function), the minimum in our situation is at 850 MeV.
- 3) $-0.1 > \delta > -1.5$, trying to be not far from the result [20].
- 4) $0.1 < w < 1$; $0.1 \text{ GeV} < m_2 < 1.5 \text{ GeV}$; $0.5 \text{ GeV} < \Lambda_1 < 2.2 \text{ GeV}$; $65 \text{ MeV} < \Lambda_2$ to provide reasonable form of the $|P_K|^2$.

To provide, for example, the condition $\delta > -0.1$, we add to χ_{restr}^2 the term

$$T = W(-\delta - 0.1 + |\delta + 0.1|)^2, \quad (6)$$

where W is the big number. So till $\delta > -0.1$ the contribution T is equal to 0, but when

$-0.1 > \delta$, T becomes large, so the minimization procedure can go outside the barrier only on a negligible distance. Our χ^2_{restr} is the sum of contributions like Eq. (6).

Using the constructed χ^2 function, we obtain Fit 6. One can see that this Fit perfectly describes the experimental data and the results based on Roy equations on the real s axis, see Table VII and Figs. 17-24. Note that in Table VII the m_{f_0} and $g_{f_0K^+K^-}^2/4\pi$ errors are adduced.

To illustrate the abilities of the background (5), we perform Fit 7 with the same resonance parameters as for Fit 3. Fit 7 provides practically the same experimental data description as Fit 3. The theoretical curves for phase δ_0^0 are shown in Fig. 25 (a), they are practically the same. It is obvious that both Fit 3 and Fit 7 provide practically identical mass spectrum in $\phi \rightarrow \pi^0\pi^0\gamma$ decay also. The inelasticity is exactly the same. Additionally, Fit 7 and Fit 3 provide indistinguishable curves for T_0^0 at $4m_\pi^2 > s > 0$, see Fig. 25 (b).

IV. CONCLUSION

Our investigation shows that the scenario, based on the four-quark model, completely agrees with the current experimental data and theoretical requirements. It is shown that the requirement of the weak $\sigma(600) - f_0(980)$ mixing leads to the $g_{\sigma K^+K^-}$ and $g_{f_0\pi^+\pi^-}$ suppression, that is predicted by the four-quark model, see Table I.

The behaviour of the factor $P_K(m)$, which corrects the kaon loop model, is model dependent. We show that for large enough $g_{f_0K^+K^-}^2/4\pi$ constant (f.e., 1.5 GeV^2) the current data (including the Ref. [10] results) may be well-described with this factor close to 1 at $850 \text{ MeV} < m$, but for smaller values of this constant (f.e., 1 GeV^2) the correction increases. New precise data on the $\pi\pi \rightarrow K\bar{K}$ reaction and the inelasticity (η_0^0) of the $\pi\pi$ scattering would give an ability to understand more about this factor and reduce the region of possible values of parameters.

The obtaining of the σ pole in Ref. [10] gave the strong argument in favor of the $\sigma(600)$ existence, but followed efforts aiming the precise determination of the pole are not productive. The Roy equations are one-channel, that is, are approximate and even slight discrepancy in the amplitude in the physical region may lead to large changes in the complex plane. Remind that the Riemannian surface of the $\pi\pi$ scattering amplitude has many sheets (strictly speaking, infinite number of sheets), and even for relatively narrow $f_0(980)$ is sometimes a

problem to determine on what sheet should we find the pole, see, for example, Fit 2 in Ref. [11]. But even if we obtained the pole precisely, it would give us practically no information on the resonance nature, because it can not be connected to coupling constant in the Hermitian (or quasi-Hermitian) Hamiltonian, see also Ref. [9], because of large imaginary part. Besides, the residue of the amplitude in the pole is strongly distorted by the background part of the amplitude, see Tables V and VI, that gives essential contribution even for relatively narrow $f_0(980)$.

Let us dwell on the results, presented in Table VI. Remind that for a stable particle with the mass m_0 there is the pole in the amplitude

$$T = -\frac{g^2/16\pi}{s - m_0^2}$$

at $s = m_0^2$, the residue of the amplitude $ResT$ is connected to the coupling constant (g) of the stable particle with the $\pi\pi$ channel.

One can see that the real part of the T_0^0 residue in the $f_0(980)$ pole is positive, so the coupling constant should be practically pure imaginary, what is physically meaningless. Note that the residue of the amplitude resonance part T_0^{0Res} is good. That is why the best way for understanding the nature of the light scalars is the investigation of their production mechanisms in physical processes.

The simple background parameterization, suggested in Sec. III, may be used for experimental data analysis and the description of the Ref. [10] results for real s . It is shown that the resonance features are practically preserved, moreover, one can see that for even more simple background, used in Ref. [1], they changed not so much, though the Ref. [10] results were not included.

In this investigation we paid more attention to the inelasticity η_0^0 , namely, we tried to reproduce the peculiar behaviour near the threshold, indicated by the experimental data. Unfortunately, the current data have large errors, so the precise measurement of the inelasticity η_0^0 near 1 GeV in $\pi\pi \rightarrow \pi\pi$ would be very important.

V. ACKNOWLEDGEMENTS

We thank very much H. Leutwyler for providing numerical values of the $T_0^0(s)$ on the real axis, obtained in Ref. [10], useful discussions, and kind contacts. This work was supported

in part by RFBR, Grant No 10-02-00016.

-
- [1] N.N. Achasov and A.V. Kiselev, Phys. Rev. **D73**, 054029 (2006); Erratum-ibid. **D74**, 059902 (2006); Yad. Fiz. **70**, 2005 (2007) [Phys. At. Nucl. **70**, 1956 (2007)].
- [2] A.Aloisio et al. (KLOE Collaboration), Phys. Lett. **B537**, 21 (2002).
- [3] N.N. Achasov and V.N. Ivanchenko, Nucl. Phys. **B315**, 465 (1989).
- [4] N.N. Achasov and V.V. Gubin, Phys. Rev. **D56**, 4084 (1997).
- [5] N.N. Achasov, V.V. Gubin, Phys. Rev. **D63**, 094007 (2001).
- [6] N.N. Achasov, Nucl. Phys. **A 728**, 425 (2003).
- [7] N.N. Achasov and A.V. Kiselev, Phys. Rev. **D68**, 014006 (2003).
- [8] N.N. Achasov and G.N. Shestakov, Phys. Rev. **D49**, 5779 (1994).
- [9] N.N. Achasov and G.N. Shestakov, Phys. Rev. Lett. **99**, 072001 (2007).
- [10] I. Caprini, G. Colangelo and H. Leutwyler, Phys. Rev. Lett. **96**, 132001 (2006).
- [11] N.N. Achasov and A.V. Kiselev, Phys. Rev. **D83**, 054008 (2011), or arXiv:1011.4446v2 [hep-ph].
- [12] R.L. Jaffe, Phys. Rev. **D15**, 267 (1977); **15**, 281 (1977).
- [13] In the kaon loop model, $\phi \rightarrow K^+K^- \rightarrow \gamma(f_0 + \sigma)$ [3–5], the amplitude of the signal $\phi(p) \rightarrow \gamma(f_0 + \sigma) \rightarrow \pi^0(k_1)\pi^0(k_2)\gamma(q)$ is
- $$M_{sig} = g(m) \left((\phi\epsilon) - \frac{(\phi q)(\epsilon p)}{(pq)} \right) T \left(K^+K^- \rightarrow \pi^0\pi^0 \right) \times 16\pi, \quad (7)$$
- where $g(m)$ is the kaon loop function, ϕ and ϵ are polarization vectors of the ϕ meson and photon, see Ref. [1, 11].
- [14] These constants are equal in the naive four-quark model.
- [15] B. Hyams et al., Nucl. Phys. **B64**, 134 (1973).
- [16] P. Estabrooks and A.D. Martin, Nucl. Phys. **B79**, 301 (1974).
- [17] A.D. Martin, E.N. Ozmütlu, E.J. Squires, Nucl. Phys. **B121**, 514 (1977).
- [18] V. Srinivasan et al., Phys. Rev. **D12**, 681 (1975).
- [19] L. Rosselet et al., Phys. Rev. **D15**, 574 (1977).
- [20] N.N. Achasov and A.A. Kozhevnikov, Phys. Rev. **D61**, 054005 (2000); Yad. Fiz. **63**, 2029 (2000) [Phys. At. Nucl. **63**, 1936 (2000)].

- [21] S. Pislak et al., Phys. Rev. Lett. **87**, 221801 (2001).
- [22] J.R. Batley et al., Eur. Phys. J. **C54**, 411 (2008).
- [23] N.N. Achasov and A.V. Kiselev, Phys. Rev. **D70**, 111901 (R) (2004).
- [24] M.N. Achasov et al, Phys. Rev. **D63**, 072002 (2001).
- [25] S.I. Dolinsky et al., Z. Phys. **C42**, 511 (1989).
- [26] M.N. Achasov et al, Phys. Lett. **B559**, 171 (2003).
- [27] I. Caprini, Phys.Rev. **D 77**, 114019 (2008).
- [28] G. Colangelo, J. Gasser and H. Leutwyler, Nucl. Phys. B 603 125 (2001).
- [29] A. Etkin et al, Phys. Rev. **D25**, 1786 (1982).